Biomass Conversion and Biorefinery (2024) 14:17041–17053
https://doi.org/10.1007/s13399-023-03907-5

ORIGINAL ARTICLE

Phyto-mediated synthesis of silver-doped zinc oxide nanoparticles from *Plectranthus barbatus* leaf extract: optical, morphological, and antibacterial properties

Adnan Alnehia[1,2] · Annas Al-Sharabi[2] · A. H. Al-Hammadi[1] · Abdel-Basit Al-Odayni[3,4] · Safiah A. Alramadhan[3,5] · Riad M. Alodeni[6]

Received: 5 November 2022 / Revised: 26 January 2023 / Accepted: 2 February 2023 / Published online: 13 February 2023

Abstract

In the present study, pristine and silver-doped zinc oxide nanoparticles (ZnO and Ag-ZnO NPs) were synthesized via a simple, eco-friendly method using a *Plectranthus barbatus* leaf aqueous extract as an NP-generating facilitator. The NPs obtained were characterized using FTIR, XRD, SEM, and UV–Vis. FTIR confirmed chemical structure, XRD emphasizes retained hexagonal crystallite structure, SEM revealed a nanosheet morphology, and optical analysis indicated bandgap improvement from 2.55 to 2.51 and 2.04 eV for pristine, 0.02, and 0.06 Ag-doped ZnO NPs. Antibacterial test, performed on *Staphylococcus aureus* and *Escherichia coli*, representing Gram-positive and Gram-negative bacteria, using the disk diffusion method in reference to azithromycin standard drug, noticeably revealed selective action for *S. aureus* with negligible activity against *E. coli*. The activity against *S. aureus* was found to be concentration- and doping-dependent, and as they increased, the activity increased as well. Such improvement in ZnO properties, as a result of certain morphology enhancement, makes it one suitable nominee for applications in various fields, such as solar cells, photocatalysis, and antibacterial applications.

Keywords Green synthesis · *Plectranthus barbatus* · Optical · Ag-doped ZnO · Antibacterial · Antibiotic · Medicinal plant

1 Introduction

Nowadays, the development of newer materials suitable for healthcare and technology involves not only selecting a material that is nontoxic and inexpensive, but also ensuring the synthesis technique is safe and cost-effective. Thus, the effort being paid by various scholars is to apply green approaches, in place of chemical and physical ones, e.g., synthesis of nanomaterials like metal and metal oxide nanoparticles (NPs). The green approach is well known for its least utilization of chemicals, requires low energy, and is low cost. It is an emerging branch of nanotechnology that provides cost-effective and eco-friendly alternatives [1].

Among metal oxides, zinc oxide (ZnO) has received special attention due to its selective activity against specific microbes [2, 3]. ZnO NPs are believed to be biosafe and biocompatible [4] for drug delivery, filling, and cosmetic [5, 6] applications; according to the US Food and Drug Administration, ZnO is classified as a nontoxic [7] material. It has considerable optical properties as well to benefit optoelectronic devices, transparent conducting, and photodegradation. It is an *n*-type semiconductor with a wide

✉ Adnan Alnehia
ad.alnehia@su.edu.ye

✉ Abdel-Basit Al-Odayni
aalodayni@ksu.edu.sa

1 Department of Physics, Faculty of Sciences, Sana'a University, 12081 Sana'a, Yemen

2 Department of Physics, Faculty of Applied Sciences, Thamar University, 87246 Dhamar, Yemen

3 Engineer Abdullah Bugshan Research Chair for Dental and Oral Rehabilitation, College of Dentistry, King Saud University, Riyadh 11545, Saudi Arabia

4 Department of Chemistry, Faculty of Education, Thamar University, 87246 Dhamar, Yemen

5 Umm Al-Momineen Maimouna Bint Al-Harth Intermediate School at the National Guard, Al Khobar Education Office, General Directorate of Education Eastern Province, Ministry of Education, Al Khobar, Saudi Arabia

6 Division of Biochemistry, Chemistry Department, Faculty of Science, Ibb University, Ibb, Yemen

optical bandgap (3.37 eV) and excessive exciton binding energy (60 meV) at room temperature [8].

It is worth mentioning that several physical and chemical techniques are available for ZnO NP synthesis. Chemical approaches include hydrothermal, precipitation, self-combustion, sol–gel, and microemulsion methods [9], etc., while high-energy ball milling, arc plasma, laser ablation, thermal evaporation, and vapor deposition methods are examples of some physical methods to synthesize ZnO NPs. However, a lot of hazardous chemicals that are not environmentally friendly are commonly used. On the other hand, biological approaches (green synthesis) are eco-friendly, safer, reproducible, and promising alternatives to physical and chemical synthesis [10]. Hence, bio-based methods for ZnO NP production such as plant-based approaches have proven to be green, simple, and inexpensive. The antibacterial activity for ZnO NPs is noteworthy high [11, 12]. Such features are associated with its low bandgap which is important for better interaction with biomolecules [5, 11]; however, their instability in water limits their biological applications [13]. Indeed, ZnO NP properties can be adjusted to a better by applying, e.g., dopants.

Doping of metal oxides provides a strategy to improve their optical, electrical, and bioactivity potentials [13–16]. The addition of a dopant during synthesis will change the crystal growth conditions, inducing internal defects and morphology changes that enhance the production of reactive oxygen species (ROS) [17]. In particular, silver (Ag) has been reported to be the best nominee for ZnO NP doping toward property enhancement including bandgap reduction and morphology change that support better antibacterial activity [8, 12, 18]. Furthermore, doping is considered a powerful tool in the development of NP functionalities by altering their structural, morphological, and chemical properties [19]. It is reported that smaller NPs have higher biological activities due to the increased surface area. The Ag-containing NP including Ag-doped ZnO NPs is one interesting biologically active material for biomedical applications and was studied for its anticancer, antimicrobial, and antioxidant; however, to gain optimal activity while maintaining a nontoxic dose, dopant concentrations must be optimized [19, 20]. In this subject, few researches on plant extract–mediated synthesis of Ag-doped ZnO NPs were reported [12, 18, 21, 22]. Studies indicated improvement in the structural, optical, and morphological properties of ZnO NPs and, as a consequence, their antibacterial activity was enhanced, thus suggesting their use in the development of the antibiotic industry and optical device applications. Currently, antibiotic resistance is one of the major clinical issues worldwide. Therefore, the development of new antimicrobial agents with more effective and promising antimicrobial properties has become very important [23]. Organic chemicals with a verity of potent heterocyclic compounds are commonly the target and are successful in developing new antimicrobials; however, a researcher lastly has proved that inorganic NPs have wide-spectrum antibacterial properties as well and, in particular, ZnO and Ag-doped were of the most promising antibiotics with tailorable properties associated with size, shape, and other physicochemical features [19].

Plectranthus barbatus is a medicinal plant used to treat a wide range of disorders including seizures [24]. Phytochemical studies on several extracts with various polarities and from different parts of the plant revealed numerous bioactive compounds that could justify its traditional uses [25]. Of these phytocompounds, forskolin is the main constituent of more than 67 isolated diterpenoids [26] and was reported as the most active against seizures [27]. In particular, aqueous leaf extract contains specific phytochemicals such as terpenoids, saponins, tannins, alkaloids, and essential oils and can be regarded as a safe medicinal plant for traditional use [28].

To the best of our knowledge, no research has been conducted on the synthesis of Ag-doped ZnO NPs using *Plectranthus barbatus* leaf extract. However, the literature indicates the implication of this plant in the phytosynthesis of pristine Ag and ZnO [29–32]. The target plant, *Plectranthus barbatus*, is a medicinal herb that belongs to the family Lamiaceae. It grows in many countries around the world such as Brazil, Egypt, India, Saudi Arabia, and Yemen and tropical East Africa as well. Furthermore, previous studies indicate its use as an antimicrobial agent [33].

Therefore, in this study, pristine and Ag-doped ZnO NPs were biosynthesized using aqueous *Plectranthus barbatus* leaf (PBL) extract and their structural, morphological, and optical properties were investigated. Moreover, the antibacterial activity of the synthesized oxides was assessed against Gram-positive and Gram-negative bacteria strains using the disk diffusion method.

2 Materials and methods

2.1 Materials

Zinc nitrate hexahydrate ($Zn(NO_3)_2{\cdot}6H_2O$; ≥ 99%), silver nitrate ($AgNO_3$; 98%), sodium hydroxide (NaOH; 98%), and ethanol (EtOH; 99.5) were procured from BDH Chemical Ltd. (Pool, England, UK). The *Staphylococcus aureus* (Gram-positive) and *Escherichia coli* (Gram-negative) test bacteria were kind gifts from Al-Jarfi Medical Lab, Dhamar, Yemen. Mueller–Hinton agar (MHA) was obtained from Sigma-Aldrich (Darmstadt, Germany). All chemicals were used as received unless stated otherwise and distilled water (dH_2O) was used wherever required.

2.2 Preparation of the aqueous leaf extract

Fresh leaves of *Plectranthus barbatus* (PBL) were collected, during the summer season of 2022, from Anis district, Dhamar governorate, Yemen. They were washed several times, severely, with tap water and distilled water; cut into small pieces; placed in a mortar; and finally ground to obtain dough mass. To prepare the extract, a weight of 16 g of this PBL dough was immersed in 250 mL dH_2O and stirred for 90 min at room temperature (RT). While mixing, the mixture changed from colorless to brown which was then filtered and immediately used for the preparation of intended NPs [11].

2.3 Green synthesis of undoped and Ag-doped ZnO NPs

In a typical procedure, an amount of 8.18 g of zinc nitrate hexahydrate salt was dissolved in 25 mL PBL aqueous extract. In a separate beaker, 4 g of NaOH was dissolved in 10 mL PBL aqueous extract and added to the metal solution to set the pH around 11. After that, the solution was magnetically stirred for 60 min at RT and then filtered and left to dry for 24 h at RT. Finally, the obtained powder was annealed at 150°C for 2 h to get undoped ZnO NPs [34, 35]. For the synthesis of Ag-doped ZnO NPs, the same procedure was carried out, with further addition of silver nitrate in a ratio equal to 2 and 6 mol% of ZnO. The overall experiments are schematically illustrated in Fig. 1.

2.4 Antibacterial test

The in vitro antibacterial activity of the biosynthesized pure ZnO and Ag-doped ZnO NPs was investigated using the well-known disk diffusion method [22, 23], against selected Gram-positive (*S. aureus*) and Gram-negative (*E. coli*) bacteria and azithromycin (AzM) as the reference standard drug [36–38]. Bacterial strains were firstly cultured at 37±1°C for 24 h and finally adjusted with nutrient broth to achieve an absorbance of 0.075–0.1. The Petri dishes containing media were prepared using MHA media over which the bacteria were spread to obtain test plates. Then, disks of 6 mm diameter, wetted by 20 µL on each side of various doses (67, 134, and 201 mg/mL) of pristine and Ag-doped ZnO NPs, were laid on the media surface and incubated at 37±1°C for 21–22 h. Disks for AzM and dH_2O were also treated similarly as samples and analyzed as positive and negative controls, respectively. The antibacterial activities were measured by a ruler and reported based on the calculated diameter of the inhibition zone (ZOI) and compared with the controls [24]. The test was performed in duplicate and the average was reported.

2.5 Characterization

FTIR spectra were obtained in a Nicolet iS10 spectrometer (Thermo-Scientific, Madison, WI, USA) using an attenuated total reflection (ATR) accessory on the range of 650–4000 cm^{-1}, being the average of 32 scans per spectrum and 4 cm^{-1} scanning resolution. The XRD profiles were collected using an XD-2 X-ray diffractometer (Beijing Purkinje General Instrument Co., Ltd., Beijing, China) with CuKα1 radiation of λ = 1.54 Å in the two-theta (2θ) degree of 15–80 and at 0.02 min^{-1}. The UV–Vis analysis was carried out using a Hitachi U-3900 UV–Vis spectrophotometer (Tokyo, Japan) on the range of 200–900 nm at RT. The surface morphology imaging was performed on a JSM-6360 LV SEM (Jeol Ltd., Tokyo, Japan) for samples sputter–coated with gold prior to application.

3 Results and discussion

3.1 FTIR analysis

The FTIR spectra of pure ZnO and 0.02 and 0.06 Ag-doped ZnO are illustrated in Fig. 2. As can be seen, the spectra share common bands over the whole screened range, i.e., the broad one on the

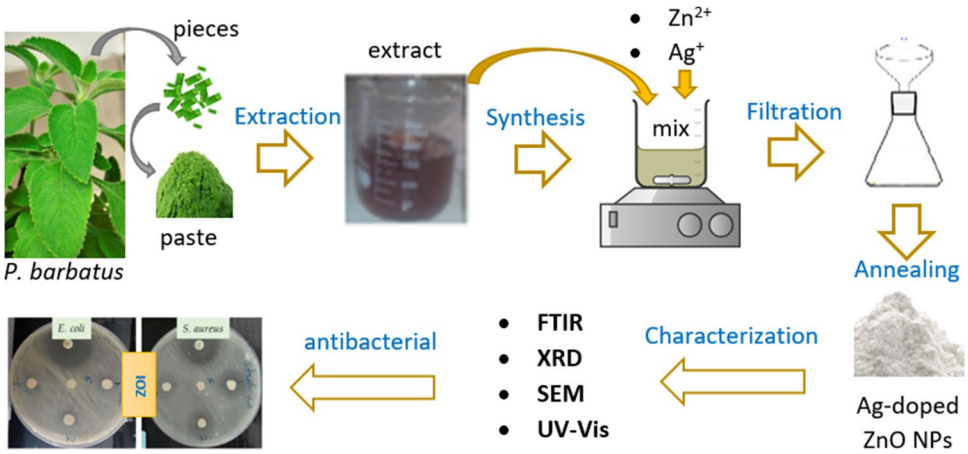

Fig. 1 Flow steps for the green synthesis of Ag-doped ZnO NPs using Plectranthus barbatus leaf extract, characterization, and antibacterial activity

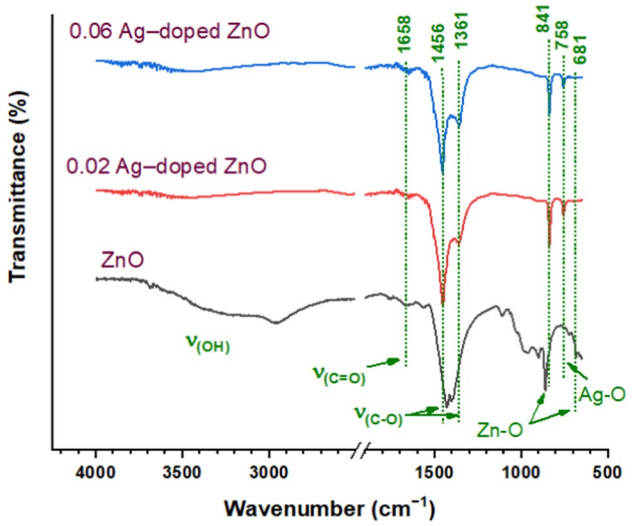

Fig. 2 FTIR spectra for pure ZnO and Ag (2, 6 mol%)-doped ZnO nanoparticles

range of 3100–3600 cm^{-1} for the stretching vibrations of metal/water molecules OH [39], the weak peak around 1658 cm^{-1}, and the strong ones at 1456 and 1361 cm^{-1} for C=O and C-O stretching vibrations [40]. However, C-O bonds can be attributed either to air background or traced plant-based organic molecules used for the preparation and stabilization of metal NPs. Additionally, the characteristic peaks of M-O NPs are usually seen on the fingerprint frequencies, i.e., below 900 cm^{-1}. However, due to the capacity limit of the ATR-FTIR device (4000–650 cm^{-1}), peaks below 650 cm^{-1} were, unfortunately, not reported. Nevertheless, the spectra are incorporated with clear peaks at 670 and 681 cm^{-1} for ZnO and at 758 cm^{-1} for Ag-O NPs, proving the formation of the intended metal oxide NPs [41].

3.2 XRD analysis

The pristine and Ag-doped ZnO NPs were characterized via powder XRD as well, to define the structure purity and crystallite size and further to study the impact of Ag on the structural properties of ZnO NPs. As shown in Fig. 3A, XRD patterns of ZnO NPs prepared using aqueous BPL extract were indexed to (100), (002), (101), (102), (110), (103), (200), (112), and (201) planes of hexagonal phase which coincide with 2θ values of 32.10, 34.76, 36.60, 47.84, 56.96, 63.24, 66.80, 68.28, and 69.46, respectively, of ZnO (JCPDS card no. 36-1451) [42], and were in good agreement with the literature [11, 43]. After doping with 2% and 6% Ag^{+}, new peaks at 38.34, 44.74, and 64.73 due to the (111), (200), and (220) of cubic phase of metallic Ag (JCPDS card no. 04-0783) were identified [44]. These peaks were very weak due to the low amount of Ag in the doped oxide. The detectable small shift in the peak positions confirms doping events as shown in Fig. 3B in which the peak at 2θ of 36.60 (101) in the undoped ZnO was shifted to 36.54 in 0.06 Ag-ZnO. The peak at $2\theta = 29.76$ might be a result of some organic materials traced from the plant.

The average crystallite size (D) of pristine and Ag-doped ZnO NPs were evaluated via Scherrer's law as well as the Williamson–Hall (W-H) methods expressed by Eqs. (1) and (2) [36, 45, 46].

$$D = \frac{0.9\lambda}{\beta\cos\theta} \tag{1}$$

$$\beta\cos\theta = \frac{0.9\lambda}{D} + 4\varepsilon\sin\theta \tag{2}$$

where θ is the diffraction angle, λ is 1.54 Å, β is full width at half maximum (FWHM), and ε is the micro-strain.

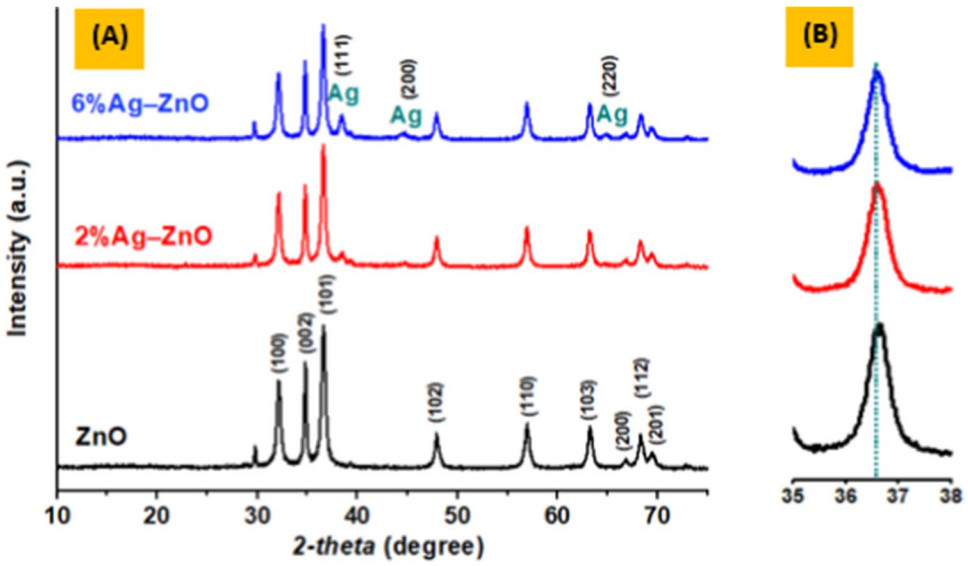

Fig. 3 **A** X-ray diffraction patterns of pure and Ag-doped ZnO NPs; **B** zoom-in representation for the prominent peak of (101) plane of synthesized NPs

Figure 4 shows the W-H diagrams for the three samples. Data obtained from XRD are summarized in Table 1. The estimated *D* values from both methods were close to each other. Broadening of the peaks in the XRD pattern obviously denotes the presence of the NPs in the prepared samples. The change in the average size after doping was due to the formation of secondary phase such as Ag and defect states.

3.3 SEM analysis

Figure 5 displays the morphology of pristine and (0.02, 0.06) Ag-doped ZnO NPs. As can be seen, the surface morphology of undoped ZnO (Fig. 5A) is very coarse and seemingly composed of agglomerated nanoplatelets with substructure as nanosheets; the thicker sheets may combine several sheets aggregated to visible larger segments with particles having irregular shapes and sizes. In Fig. 5B, C, the morphology of the Ag-doped ZnO NPs is less agglomerate, with a curly hair-like structure having a diameter in the tenth of nanoscale and lengths of less than a micrometer; however, their structures are more regular and less aggregate than pure ZnO. Furthermore, nano-stick-like structures were also observed, more visible in doped ZnO materials, indicating that Ag influences the morphology of the synthesized samples [2, 47]. As could be seen, particle sizes are seemingly smaller for doped material, and furthermore, morphology is accompanied with certain voids that may play a vital role in the antibacterial activity enhancement [48].

3.4 Optical analysis

UV–visible spectroscopy was employed to study the optical properties of the prepared NPs. The spectra of the as-prepared pure, 0.02Ag-, and 0.06Ag-doped ZnO NPs are given in Fig. 6A, showing their absorption edges at 256, 279, and 291 nm, respectively. It could be seen that as Ag doping ratio increases, the absorption edge shifts toward a higher

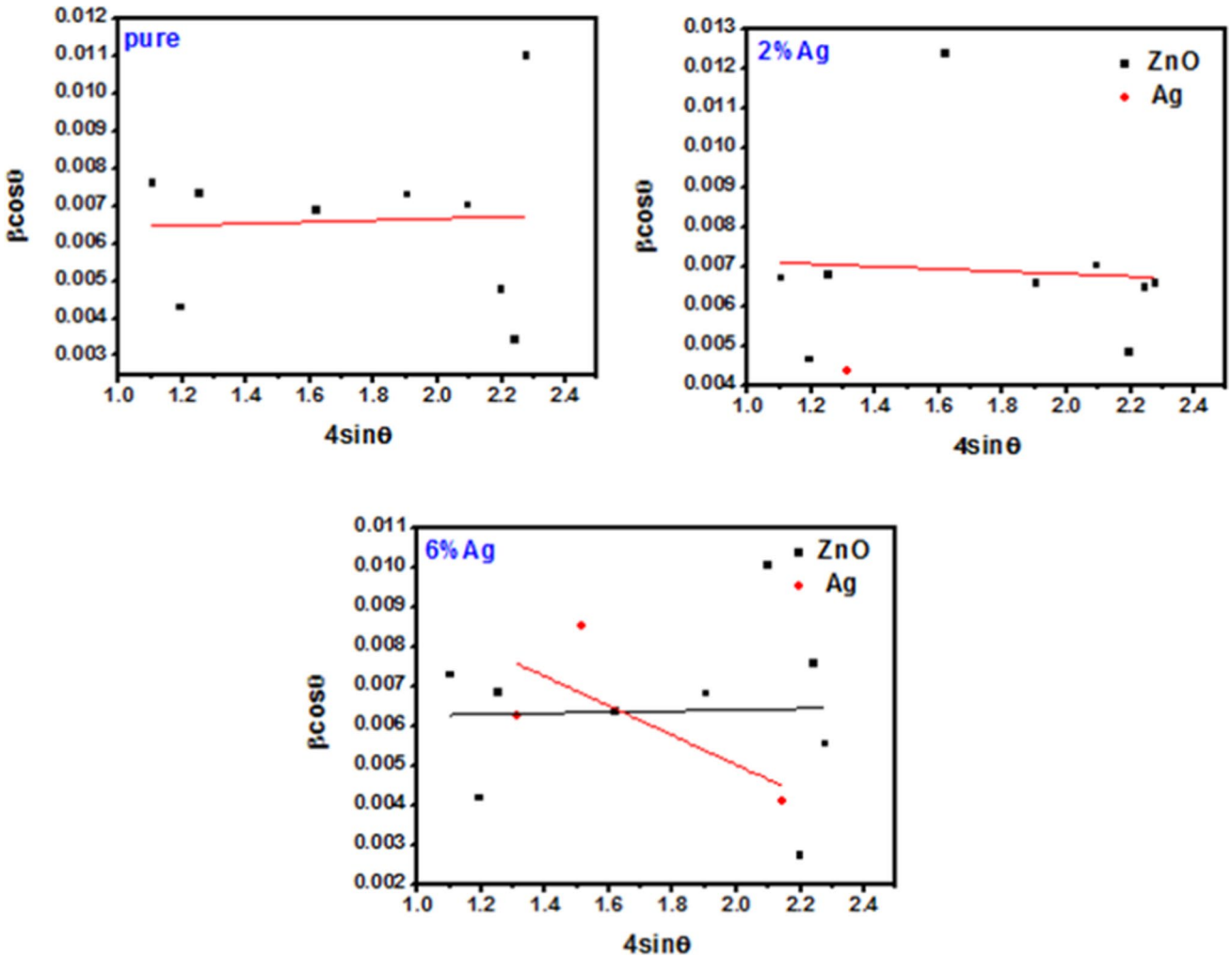

Fig. 4 The W-H method of pure ZnO and Ag (2, 6%)-doped ZnO NPs

Table 1 Structural parameters of ZnO and Ag-doped ZnO NPs

Sample	Phase ID	2-theta	*hkl*	*d*-spacing (Å)	FWHM	Crystallite size *D* (nm)	Average *D* (nm)	
							Scherrer method	W-H method
Pure ZnO	ZnO	32.10	100	2.7861	0.452	18.29	23.44	22.35
		34.76	002	2.5786	0.257	32.39		
		36.60	101	2.4531	0.441	18.97		
		47.84	102	1.8997	0.431	20.16		
		56.96	110	1.6154	0.474	19.06		
		63.24	103	1.4692	0.471	19.80		
		66.80	200	1.3993	0.326	29.18		
		68.28	112	1.3725	0.237	40.49		
		69.46	201	1.3521	0.765	12.63		
2% Ag: ZnO	ZnO	32.14	100	2.7828	0.399	20.72	21.61	18.65
		34.76	002	2.5787	0.278	29.95		
		36.56	101	2.4558	0.409	20.46		
		47.84	102	1.8997	0.775	11.21		
		56.92	110	1.6164	0.428	21.11		
		63.20	103	1.4701	0.472	19.76		
		66.68	200	1.4015	0.331	28.73		
		68.32	112	1.3718	0.447	21.48		
		69.46	201	1.3520	0.458	21.10		
	Ag	38.34	111	2.3455	0.264	31.86	31.86	-
6% Ag: ZnO	ZnO	32.08	100	2.7877	0.434	19.05	24.78	22.68
		34.74	002	2.5802	0.250	33.29		
		36.54	101	2.4570	0.412	20.31		
		47.84	102	1.8997	0.398	21.84		
		56.90	110	1.6169	0.443	20.39		
		63.26	103	1.4688	0.676	13.80		
		66.72	200	1.4008	0.186	51.13		
		68.28	112	1.3725	0.524	18.31		
		69.44	201	1.3524	0.386	25.04		
	Ag	38.44	111	2.3399	0.380	22.14	24.18	11.15
		44.54	200	2.0325	0.526	16.32		
		64.80	220	1.4376	0.276	34.08		

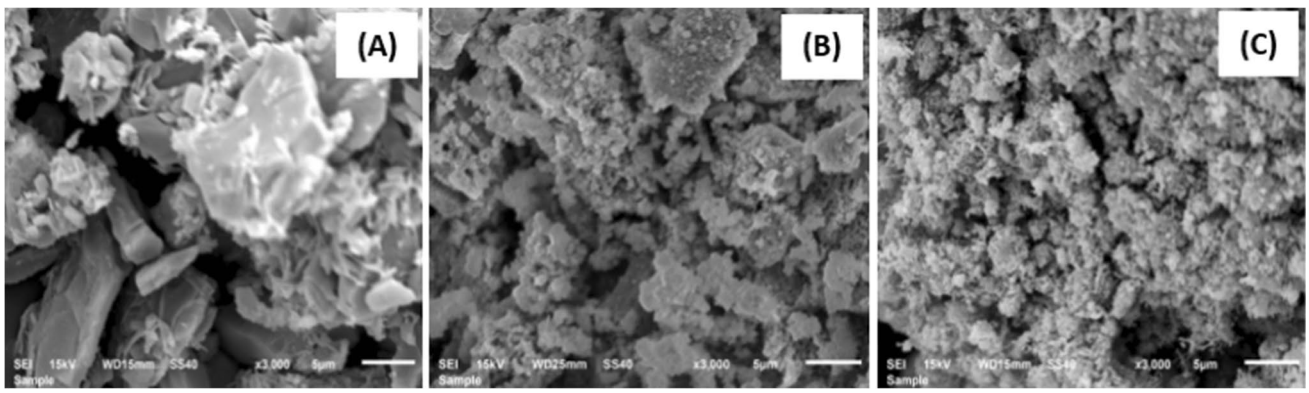

Fig. 5 SEM images for **A** pristine, **B** 0.02Ag-doped ZnO NPs, and **C** 0.06Ag-doped ZnO NPs

wavelength, indicating capacity increase as Ag concentration increases. The coefficient of absorption (α) can be computed via Eq. (3) [49].

$$\alpha = -\frac{\ln(T)}{t} = \frac{2.303A}{t} \tag{3}$$

where T, A, and t are transmittance, absorption, and thickness, respectively. Figure 6B depicting α values as a function of wavelength reveals that α is decreased as λ increased, and such reduction might be a result of charge carrier's inelastic scattering by phonons. The higher values of the coefficient of absorption in the UV region for NPs are due to the transition between extended states in the valence band (VC) and conduction band (CB). Moreover, the existence of the absorption edge in the UV region revealed that the grown NPs are appropriate for photonic applications [50].

The coefficient of extinction (k) and refractive index (n) were computed from the coefficient of absorption (α) and reflectance (R), following Eqs. (4) and (5) [37, 51, 52], respectively.

$$k = \frac{\alpha\lambda}{4\pi} \tag{4}$$

$$n = \frac{1 + R^{0.5}}{1 - R^{0.5}} \tag{5}$$

As shown in Fig. 6C, the increase in k values was seen at the lower wavelength then, as the wavelength increases, k decreases to a certain point beyond which the k gradually increased as the wavelength increased. Figure 6D displays the optical refractive index (n) of the sample under investigation that is higher at a lower wavelength, decreased upward at the UV region, and becomes constant at the visible region for all the prepared samples.

The optical conductivity (σ_{opt}) is one another important property to be assessed, which depends on the α, n, and

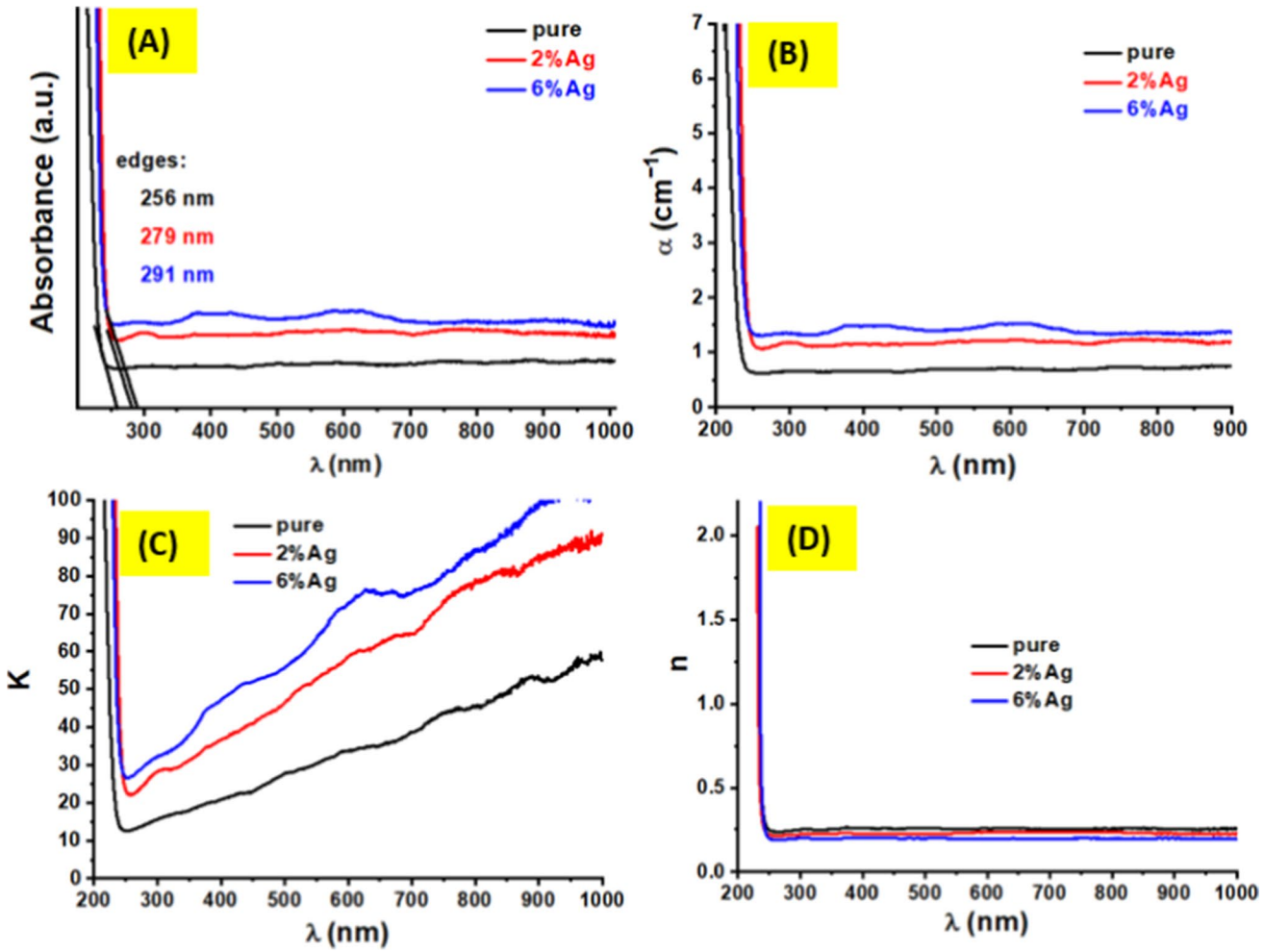

Fig. 6 **A** Absorption spectra, **B** absorption coefficient (α), **C** extinction coefficient (k), and **D** refractive index (n) of pure ZnO and Ag (2, 6%)-doped ZnO NPs

speed of light (c) as given in Eq. (6) [53]. As could be seen in Fig. 7, the change in the σ_{opt} of grown NPs possesses a maximum value in the low wavelength regions which specify that the prepared materials can be employed in optical and electronic applications.

$$\sigma_{opt} = \frac{\alpha\lambda c}{4\pi} \tag{6}$$

The real (ε_r) and imaginary (ε_i) parts of dielectric constants can be calculated using Eqs. (7) and (8) [54].

$$\varepsilon_r = n^2 - k^2 \tag{7}$$

$$\varepsilon_i = 2nk \tag{8}$$

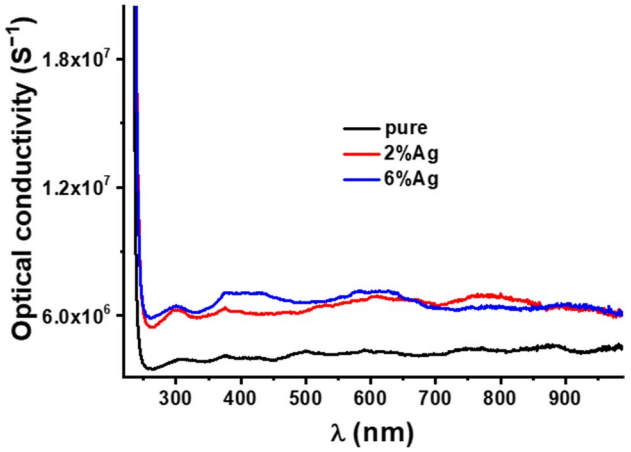

Fig. 7 Optical conductivity as a function of wavelength for pure and Ag-doped ZnO samples

Figure 8A, B displays the variation in the ε_i and ε_r for samples under investigation, showing that the ε_r was exponentially increased as photon energy ($h\nu$) increased, then sharply decreased, confirming the free carrier's contribution to the absorption, while ε_i was increased at the higher energy region. Moreover, the results illustrated that the behavior of ε_r and ε_i depends on interactions through electrons and photons with the wavelength.

The optical bandgap (E_g) of pristine and Ag-doped ZnO NPs were evaluated by Tauc's formula, Eq. (9).

$$\alpha h\nu = D\left(h\nu - E_g\right)^m \tag{9}$$

where α is the coefficient of absorption, D is a constant, m (the exponential) is a type of transition, and $h\nu$ is the energy of the photon [45, 55, 56]. From Tauc's plot (Fig. 9), the E_g values were seen to be reduced with doping increase. The E_g value of pure was 2.55 eV, and with doping of Ag in the zinc oxide lattice, the bandgap was decreased to 2.51 and 2.04 eV for 2% and 6% Ag-doped ZnO NPs, respectively, a result that agrees with the literature [35]. The red shift in the E_g could be a result of one or more reasons like the generation of new energy states between the valance and conduction bands, the effect of original defects that produce local electronic states within the energy gap [57, 58], and the variation in the ionic radius (ionic radius Ag: 1.15Å and ionic radius Zn: 0.74 Å) [6, 55]. Such red shift in the E_g after doping has proven the benefit of the doping process for NP property enhancement.

3.5 Antibacterial activity

The antibacterial activity of pristine and Ag-doped ZnO NPs prepared using *PBL* aqueous extract was analyzed against

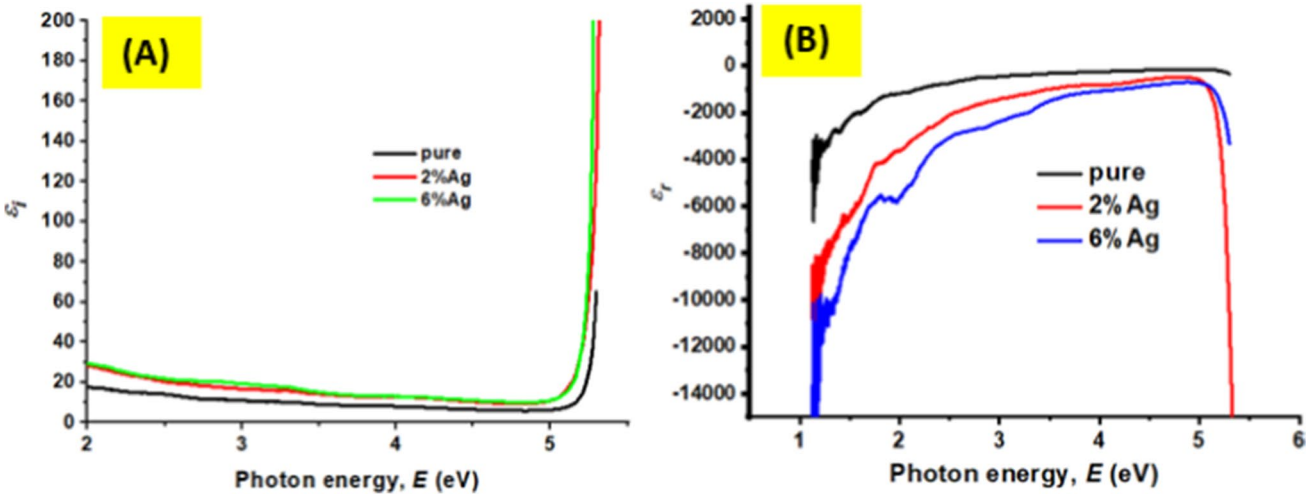

Fig. 8 **A** Imaginary (ε_i) and **B** real (ε_r) dielectric constants as a function of the photon energy of pure ZnO and Ag (2, 6%)-doped ZnO NPs

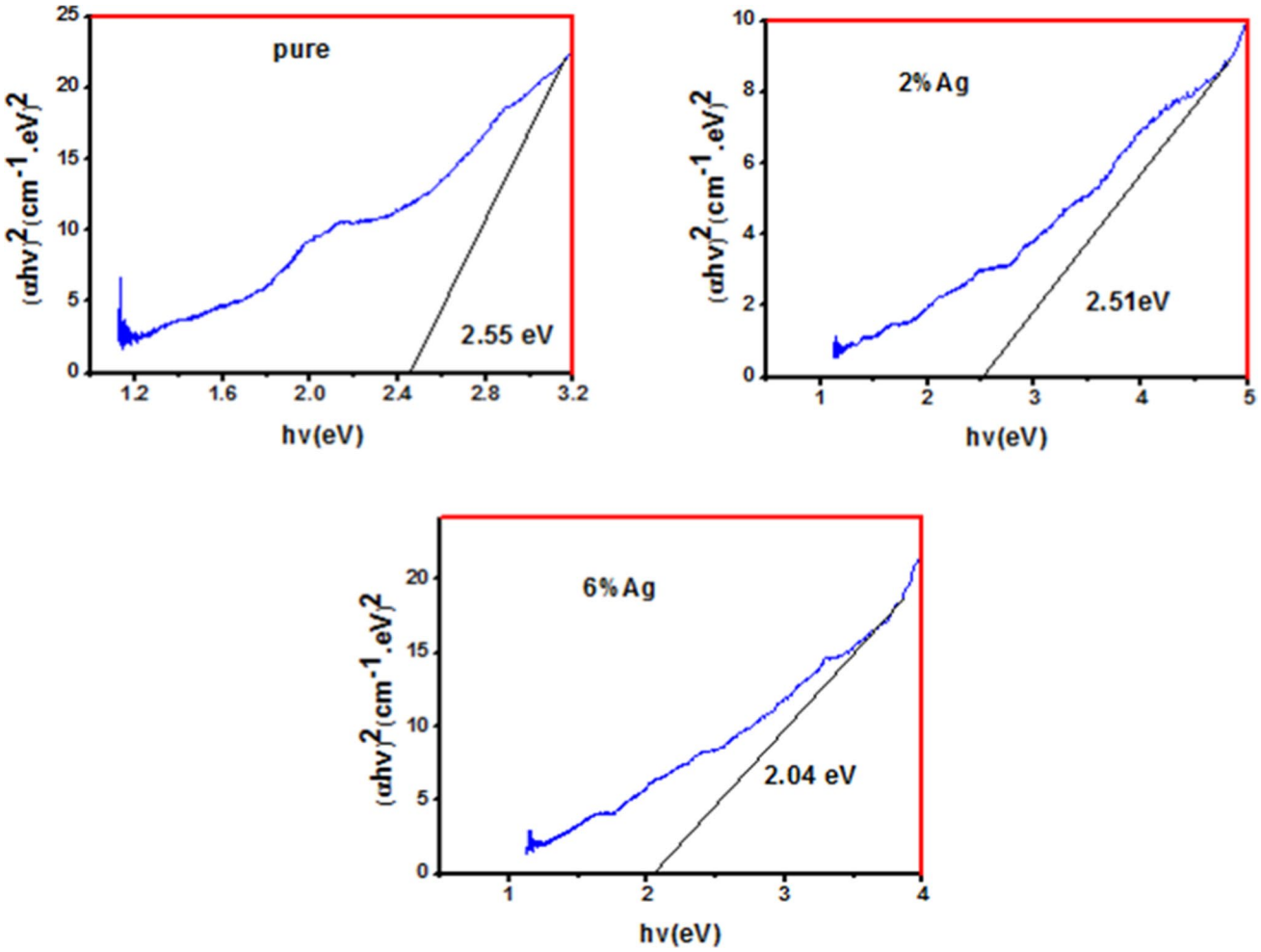

Fig. 9 The optical energy gap of pure ZnO and Ag (2, 6%)-doped ZnO nanoparticles

Gram-positive (*S. aureus*) and Gram-negative (*E. coli*) bacteria using the paper-disk diffusion method. The data obtained for ZOI of the investigated samples (ZnO, 0.02Ag-ZnO, and 0.06Ag-ZnO) at concentrations of 67, 134, and 201 mg/mL is illustrated in Fig. 10, and selected plate images for the experimental tests are given in Fig. 11; here, as the observed inhibitory effect against *E. coli* is seemingly insignificant (Fig. 11), Fig. 10 represents only *S. aureus*. According to the results, the antibacterial potency was improved after doping, with ZOI increased as the doping percentage as well as the NP concentration increased. Such improvement may be a result of crystal-shaped defects caused by doping. Furthermore, studies revealed a big impact of the NP size in their bioactivity action and found that the smaller the particle size the more activity against bacteria due to their high surface area to bound bacteria [19, 59]. It is worth noting that small-sized NPs can interact with cell membranes more efficiently than larger ones, thus working toward growth inhibition by modifying the lipid bilayer, promoting permeability, and finally causing cell death. Additionally, it is proven that NPs interact with microbes in a

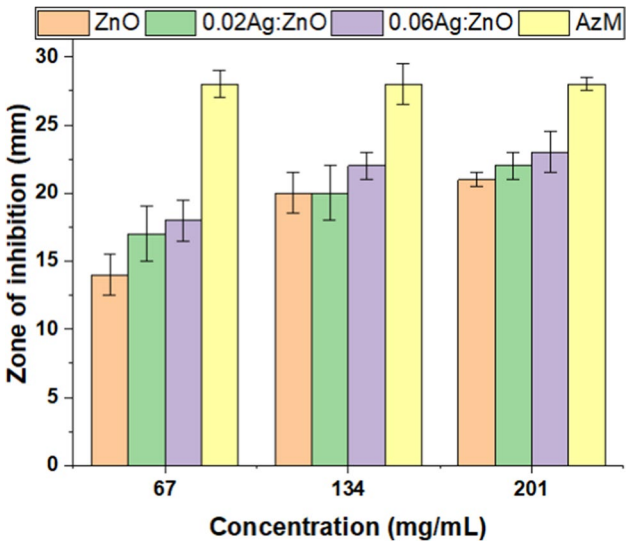

Fig. 10 Histogram illustration for the zone of inhibition of pristine and Ag-doped ZnO NPs against S. aureus. Bars represent the standard deviation of two experiments

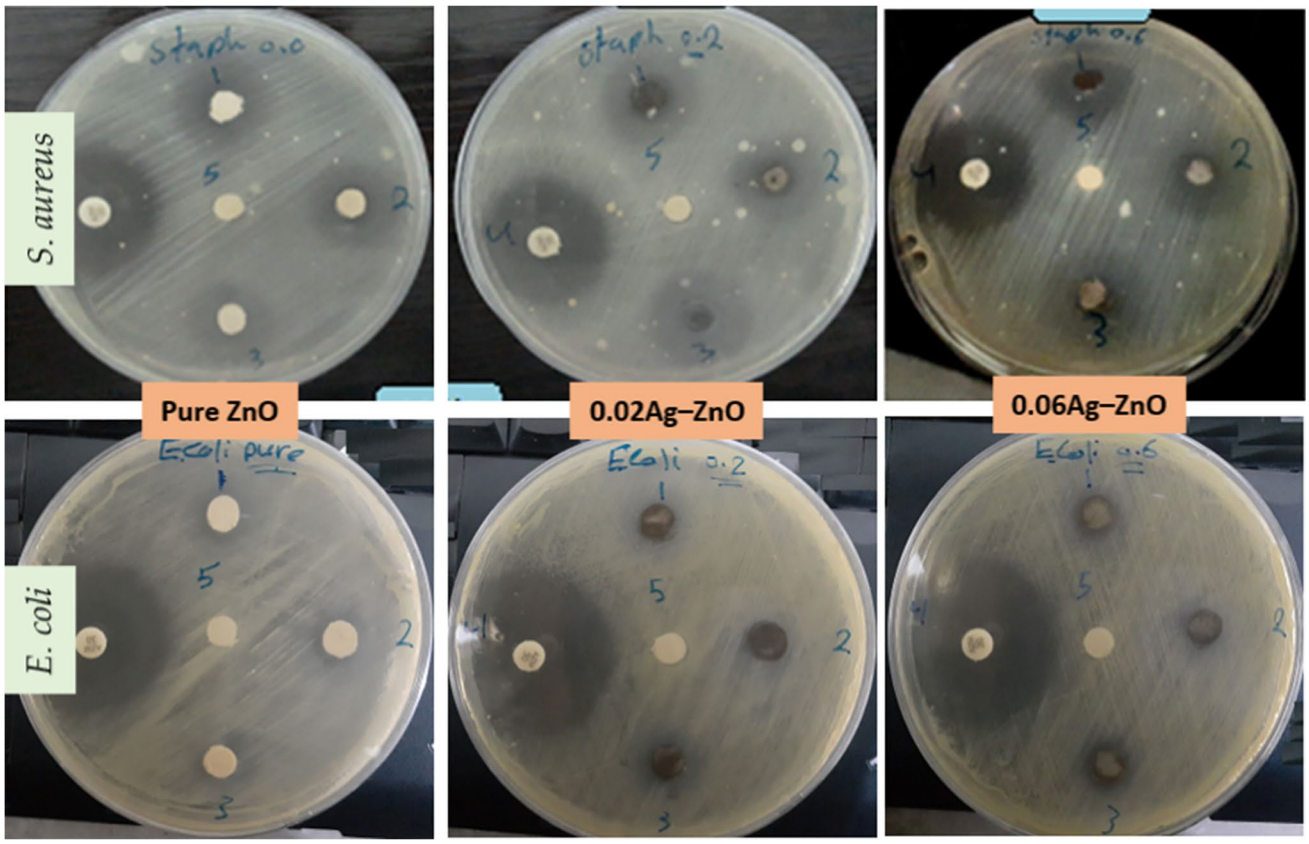

Fig. 11 Selected plates for antibacterial activity experiments of pure, 2% Ag-, and 6% Ag-doped ZnO NPs against Gram-positive bacteria (S. aureus) and Gram-negative bacteria (E. coli). Disks: (1) 67 mg/mL, (2) 134 mg/mL, and (3) 201 mg/mL per disk; (4) azithromycin antibiotics (positive control); and (5) distilled water (negative control)

particle shape-dependent manner as well [60]. By increasing dopant concentration, shape defect may increase, leading to a certain activity, i.e., antibacterial increase as shown in Fig. 10. With NP concentration increase, the number of antibacterial acting agents in the media increases, thus expecting higher activity. Accordingly, various parameters may influence the antibacterial activity of ZnO NPs, including doping ratio, NP sizes, NP shapes, and the bacteria type and environment-related conditions. The doping degree may have less effect after a certain amount as the difference becomes less between 0.02 and 0.06% compared with that between pure ZnO and 0.02% doped one (Fig. 10). In addition, the obtained results, along with those of previous studies, demonstrate that doping of Ag on ZnO NPs reduces the bandgap energy by enhancing electron-hole charge separation which further drives antibacterial increase [61]. Such mechanism may define the indirect relationship between bandgap and antibacterial activity. As seen in Fig. 11, the effect of NPs was more pronounced with *S. aureus* (Gram-positive) than *E. coli* (Gram-negative) bacteria, a result that agrees with some reported researches [62–64]. However, the mechanism behind this behavior is rather complex and more research is needed to resolve this issue. On the one hand, as the inhibition of bacterial growth is drug concentration–dependent, the applied concentration may still be below the minimum inhibitory concentration against *E. coli*. On the other hand, it could be a metabolism-dependent action as bacteria can metabolize metal ions (ca. Zn^{2+}, Ag^{+}) as an oligo-element, revealing nontoxic ZnO (or Ag-doped ZnO) for *E. coli* up to 201 mg/mL [64]. It is known that Gram-negative bacteria are less susceptible to antibacterial potency than Gram-positive ones, and this is common to their cell-wall structure differences [35, 41, 65].

Meanwhile, the antibacterial activity of a certain type of NPs depends on a number of factors such as particle size and shape, surface charge, concentration, and exposure time; the destructive action could undergo one or simultaneous mechanisms that could briefly be listed as (i) attachment of bioactive agent to the microorganism surface leading to membrane morphology change, damaging, component leakage, and finally functionality loss [66]; (ii) release of metal ions (i.e., Zn^{2+}, Ag^{+}) that, upon penetration, can inhibit several essential cell activities, resulting in cell death [43]; and (iii) generation of reactive oxygen species (ROS) which cause cell oxidative stress and later on cell damage [67, 68].

4 Conclusion

In this study, pure and Ag (2% and 6%)-doped ZnO NPs were successfully fabricated by a green route using *PBL* extract at room temperature. FTIR affirmed material structure. XRD has proven NP production with a hexagonal crystallite structure. SEM images indicated the variation in the morphology between pristine and Ag-doped ZnO. UV–Vis spectrum displayed a decrease in the material bandgaps after doping, thus supporting their potential application for optoelectronics. Antibacterial tests revealed material-concentration–dependent activity, noticeably selective against *S. aureus* (Gram-positive bacteria) than *E. coli* (Gram-negative bacteria), increased with concentration and degree of doping. Therefore, such enhanced activity for the prepared pristine ZnO and its Ag-doped NPs makes them suitable nominees for antibiotic development toward its application in healthcare and biotechnology.

Acknowledgements The authors extend their appreciation to the Deputyship for Research & Innovation, Ministry of Education in Saudi Arabia, for funding this research work through project no. IFKSURG-2-1509. The authors would like to thank Dr. Abdullah Al-Jarfi (Al-Jarfi Medical Lab) for his sincere assistance with the biology tests.

Author contribution Conceptualization: Adnan Alnehia, Annas Al-Sharabi, and A.H. Al-Hammadi. Methodology: Adnan Alnehia and Riad M. Alodeni. Formal analysis and investigation: Adnan Alnehia, Abdel-Basit Al-Odayni, and Safiah A. Alramadhan. Writing—original draft preparation: Adnan Alnehia and Abdel-Basit Al-Odayni. Writing—review and editing: Adnan Alnehia and Abdel-Basit Al-Odayni. Visualization: Adnan Alnehia and Abdel-Basit Al-Odayni. Supervision: Annas Al-Sharabi, A.H. Al-Hammadi.

Data availability The data used to support the finding of this study is included in the manuscript.

Declarations

Ethics approval Not applicable.

Competing interests The authors declare no competing interests.

References

1. Ubaithulla BA, Vadamalar R, Vinodhini A, Fairose S, Gomathiyalini A, Jabena BN, Jabeen S (2020) Facile green synthesis of silver doped ZnO nanoparticles using Tridax procumbens leaf extract and their evaluation of antibacterial activity. J Water Environ Nanotechnol (JWENT) 5:307
2. Jabeen S (2020) Facile green synthesis of silver doped ZnO nanoparticles using Tridax procumbens leaf extract and their evaluation of antibacterial activity, Journal of Water and Environmental. Nanotechnology 5:307–320
3. Elumalai K, Velmurugan S, Ravi S, Kathiravan V, Raj GA (2015) Bio-approach: plant mediated synthesis of ZnO nanoparticles and their catalytic reduction of methylene blue and antimicrobial activity. Adv Powder Technol 26:1639–1651
4. Zhou J, Xu NS, Wang ZL (2006) Dissolving behavior and stability of ZnO wires in biofluids: a study on biodegradability and biocompatibility of ZnO nanostructures. Adv Mater 18:2432–2435
5. Shabaani M, Rahaiee S, Zare M, Jafari SM (2020) Green synthesis of ZnO nanoparticles using loquat seed extract; biological functions and photocatalytic degradation properties. LWT 134:110133
6. Chen H, Qu Y, Sun L, Peng J, Ding J (2019) Band structures and optical properties of Ag and Al co-doped ZnO by experimental and theoretic calculation Physica E: Low-dimensional. Syst Nanostructures 114:113602
7. Vijayakumar S, Mahadevan S, Arulmozhi P, Sriram S, Praseetha P (2018) Green synthesis of zinc oxide nanoparticles using Atalantia monophylla leaf extracts: characterization and antimicrobial analysis. Mater Sci Semiconductor Proc 82:39–45
8. Rohith NM, Kathirvel P, Saravanakumar S, Mohan L (2018) Influence of Ag doping on the structural, optical, morphological and conductivity characteristics of ZnO nanorods. Optik 172:940–952
9. Kołodziejczak-Radzimska A, Jesionowski T (2014) Zinc oxide—from synthesis to application: a review. Materials 7:2833–2881
10. Agarwal H, Menon S, Kumar SV, Rajeshkumar S (2018) Mechanistic study on antibacterial action of zinc oxide nanoparticles synthesized using green route. Chemico-biological interactions 286:60–70
11. Khan MM, Harunsani MH, Tan AL, Hojamberdiev M, Poi YA, Ahmad N (2020) Antibacterial studies of ZnO and Cu-doped ZnO nanoparticles synthesized using aqueous leaf extract of Stachytarpheta jamaicensis. BioNanoScience 10:1037–1048
12. Saravanadevi K, Kavitha M, Karpagavinayagam P, Saminathan K, Vedhi C (2022) Biosynthesis of ZnO and Ag doped ZnO nanoparticles from Vitis vinifera leaf for antibacterial, photocatalytic application. Mater Today: Proc 48:352–356
13. da Silva BL, Abuçafy MP, Manaia EB, Junior JAO, Chiari-Andréo BG, Pietro RCR, Chiavacci LA (2019) Relationship between structure and antimicrobial activity of zinc oxide nanoparticles: an overview. Intl J Nanomed 14:9395
14. Dobrucka R, Dugaszewska J (2016) Biosynthesis and antibacterial activity of ZnO nanoparticles using Trifolium pratense flower extract. J Biol Sci 23:517–523
15. Gawade VV, Gavade NL, Shinde HM, Babar SB, Kadam AN, Garadkar KM (2017) Green synthesis of ZnO nanoparticles by using Calotropis procera leaves for the photodegradation of methyl orange. Mater Sci Mater Electron 28:14033–14039
16. Ba-Abbad MM, Takriff MS (2017) Abdelbaki Benamor Ebrahim Mahmoudi, Abdul Wahab Mohammad, Arabic gum as green agent for ZnO nanoparticles synthesis: properties, mechanism and antibacterial activity, Materials Science. Mater Electron 28:12100–12107
17. Bomila R, Suresh S, Srinivasan S (2019) Synthesis, characterization and comparative studies of dual doped ZnO nanoparticles for photocatalytic applications. J Mater Sci Mater Electron 30:582–592
18. Sharma M, Bassi H, Chauhan P, Thakur P, Chauhan A, Kumar R, Kollarigowda RH, Thaku NK (2022) Inhibition of the bacterial growth as a consequence of synergism of Ag and ZnO: Calendula officinalis mediated green approach for nanoparticles and impact of altitude. Inorganic Chem Commun 136:109131
19. Shinde RS, More RA, Adole VA, Koli PB, Pawar TB, Jagdale BS, Desale BS, Sarnikar YP (2021) Design, fabrication, antitubercular, antibacterial, antifungal and antioxidant study of silver doped ZnO and CuO nano candidates: a comparative pharmacological study. Curr Res Green Sust Chem 4:100138
20. Magar MH, Adole VA, Waghchaure RH, Pawar TB (2022) Efficient photocatalytic degradation of eosin blue dye and antibacterial study using nanostructured zinc oxide and nickel modified zinc oxide. Res Chem 4:100537
21. Khatir NM, Sabbagh F (2022) Green facile synthesis of silver-doped zinc oxide nanoparticles and evaluation of their effect on drug release. Materials 15:5536

22. Mthana MS, Mthiyane MN, Ekennia AC, Singh M, Onwudiwe DC (2022) Cytotoxicity and antibacterial effects of silver doped zinc oxide nanoparticles prepared using fruit extract of Capsicum Chinense. Scientific African 17:e01365
23. Adole VA, More RA, Jagdale BS, Pawar TB, Chobe SS, Shinde RA, Dhonnar SL, Koli PB, Patil AV, Bukane AR (2021) Microwave prompted solvent-free synthesis of new series of heterocyclic tagged 7-arylidene indanone hybrids and their computational, antifungal, antioxidant, and cytotoxicity study. Bioorganic Chem 115:105259
24. Borges Fernandes LC, Campos Câmara C, Soto-Blanco B (2012) Anticonvulsant activity of extracts of *Plectranthus barbatus* leaves in mice. Evid Based Complement Alternat Med 2012:1–4
25. Alasbahi RH, Melzig MF (2010) Plectranthus barbatus: a review of phytochemistry, ethnobotanical uses and pharmacology–part 2. Planta medica 76:753–765
26. Cordeiro M, Nunes T, Bezerra F, Damasco P, Silva W, Ferreira M, Magalhães O, Soares L, Cavalcanti I, Pitta M (2021) Phytochemical characterization and biological activities of *Plectranthus barbatus* Andrews. Braz J Biol 82:e236297
27. Valdes L, Mislankar S, Paul A (1987) Coleus barbatus (C. forskohlii)(Lamiaceae) and the potential new drug forskolin (Coleonol). Economic botany 41:474–483
28. Ezeonwumelu JO, Kawooya GN, Okoruwa AG, Dare SS, Ebosie JC, Akunne AA, Tanayen JK, Udechukwu BE (2019) Phytochemical screening, toxicity, analgesic and anti-pyretic studies of aqueous leaf extract of Plectranthus barbatus [Andrews. Engl.] in rats. Pharmacol Pharm 10:205
29. Chandraker SK, Lal M, Ghosh MK, Ram T, Paliwal R, Shukla R (2022) Biofabrication of spherical silver nanoparticles using leaf extract of Plectranthus barbatus Andrews: characterization, free radical scavenging, and optical properties. Inorganic Chem Commun 142:109669
30. Vijayakumar S, Malaikozhundan B, Shanthi S, Vaseeharan B, Thajuddin N (2017) Control of biofilm forming clinically important bacteria by green synthesized ZnO nanoparticles and its ecotoxicity on Ceriodaphnia cornuta. Microbial Pathogenesis 107:88–97
31. Aswathy B, Vishnudasan D, Manoj P (2021) Bio-synthesis, characterization and antibacterial studies of ZnO nanoparticles. International Journal of Materials Research 112:963–968
32. Masalu R, Ngassa S, Kinunda G, Mpinda C (2020) Antibacterial and anti-HIV-1 reverse transcriptase activities of selected medicinal plants and their synthesized zinc oxide nanoparticles, Tanzania Journal of. Science 46:597–612
33. Almeida WAd, Nova ICV, Nascimento JdS, Moura MCd, Agra-Neto AC, Costa HNd, Cruz GdS, Teixeira AAC, Wanderley-Teixeira V, Ferreira MRA, Soares LAL, Coelho LCBB, MariaNavarro DF, Paiva PMG, Napole TH, Albuquerque LPd, Pontual EV (2021) Effects of Plectranthus barbatus leaf extract on survival, digestive proteases, midgut morphophysiology and gut microbiota homeostasis of Aedes aegypti larvae, South African. J Bot 141:116-125
34. Khan MM, Harunsani MH, Tan AL, Hojamberdiev M, Azamay S, Ahmad N (2020) Antibacterial activities of zinc oxide and Mn-doped zinc oxide synthesized using Melastoma malabathricum (L) leaf extract. Bioprocess Biosyst Eng 43:1499–1508
35. Alnehia A, Al-Odayni A-B, Al-Sharabi A, Al-Hammadi A, Saeed WS (2022) Pomegranate peel extract-mediated green synthesis of ZnO-NPs: extract concentration-dependent structure, optical, and antibacterial activity. J Chem 2022:1–11. https://doi.org/10.1155/2022/9647793
36. Hezma AM, Rajeh A, Mannaa MA (2019) An insight into the effect of zinc oxide nanoparticles on the structural, thermal, mechanical properties and antimicrobial activity of Cs/PVA composite. Colloids and Surfaces A 581:123821
37. Al-Sharabi A, Sada'a KSS, AL-Osta A, Abd-Shukor R (2022) Structure, optical properties and antimicrobial activities of MgO–$Bi_{2-x}Cr_xO$ nanocomposites prepared via solvent-deicient method. Sci Rep 12:10647
38. Saif MMS, Alodeni RM, Alghamdi AA, Al-Odayni A-B (2022) Synthesis, spectroscopic characterization, thermal analysis and in vitro bioactivity studies of the N-(cinnamylidene) tryptophan Schiff base. J King Saud University-Science 34:101988
39. Saleem S, Jameel MH, Akhtar N, Nazir N, Ali A, Zaman A, Rehman A, Butt S, Sultana F, Mushtaq M (2022) Modification in structural, optical, morphological, and electrical properties of zinc oxide (ZnO) nanoparticles (NPs) by metal (Ni, Co) dopants for electronic device applications. Arab J Chem 15:103518
40. Ramesan M, Greeshma K, Parvathi K, Anilkumar T (2020) Structural, electrical, thermal, and gas sensing properties of new conductive blend nanocomposites based on polypyrrole/phenothiazine/silver-doped zinc oxide. J Vinyl and Additive Technol 26:187–195
41. Naseer M, Aslam U, Khalid B, Chen B (2020) Green route to synthesize zinc oxide nanoparticles using leaf extracts of Cassia fistula and Melia azadarach and their antibacterial potential. Sci Rep 10:1–10
42. Moulahi A (2021) Efficient photocatalytic performance of Mg doping ZnO for the photodegradation of the rhodamine B. Inorganic Chem Commun 133:108906
43. Alnehia A, Al-Hammadi AH, Al-Sharabi A, Alnahari H (2022) Optical, structural and morphological properties of ZnO and Fe+3 doped ZnO-NPs prepared by Foeniculum vulgare extract as capping agent for optoelectronic applications Inorganic. Chem Commun 143:109699
44. Femi-Adepoju AG, Dada AO, Otun KO, Adepoju AO, Fatoba OP (2019) Green synthesis of silver nanoparticles using terrestrial fern (Gleichenia Pectinata (Willd) C Presl): characterization and antimicrobial studies. Heliyon 5:01543
45. Alwany AB, Youssef GM, Saleh EE, Samir OM, Algradee MA, Alnehia A (2022) Structural, optical and radiation shielding properties of ZnS nanoparticles QDs Optik. Intl J for Light and Electron Optics 260:169124
46. Ismail MA, Taha K.K, Modwi A, Khezami L (2018) ZnO nanoparticles: surface and X-ray profile analysis. J Ovonic Res 14:381-393
47. Pandiyan N, Murugesan B, Arumugam M, Sonamuthu J, Samayanan S, Mahalingam S (2019) Ionic liquid-a greener templating agent with Justicia adhatoda plant extract assisted green synthesis of morphologically improved Ag-Au/ZnO nanostructure and it's antibacterial and anticancer activities. J Photochem Photobiol Biol 198:111559
48. Brown D (2015) Antibiotic resistance breakers: can repurposed drugs fill the antibiotic discovery void? Nat Rev Drug Dis 14:821–832
49. Mukhtar F, Munawar T, Nadeem MS, Rehman MNu, Riaz M, Iqbal F (2021) Dual S-scheme heterojunction ZnO–V_2O_5–WO nanocomposite with enhanced photocatalytic and antimicrobial activity. Mater Chem Phys 263:124372
50. Zak AK, Abrishami ME, Majid WA, Yousefi R, Hosseini S (2011) Effects of annealing temperature on some structural and optical properties of ZnO nanoparticles prepared by a modified sol–gel combustion method. Ceramics Intl 37:393–398
51. Nadeem MS, Munawar T, Mukhtar F, Rahman MNu, Riaz M, Hussain A, Iqbal F (2020) Hydrothermally derived co, Ni co-doped ZnO nanorods; structural, optical, and morphological study. Opt Mater 111:110606
52. Abdulwahab A, Al-Mahdi EA, Al-Osta A, Qaid A (2021) Structural, optical and electrical properties of CuSCN nano-powders doped with Li for optoelectronic applications. Chinese J Phys 73:479–492

53. Munawar T, Iqbal F, Yasmeen S, Mahmood K, Hussain A (2020) Multi metal oxide NiO-CdO-ZnO nanocomposite–synthesis, structural, optical, electrical properties and enhanced sunlight driven photocatalytic activity. Ceramics Intl 46:2421–2437
54. Azmand A, Kafashan H (2019) Al-doped ZnS thin films: physical and electrochemical characterizations. J\ Alloys Com 779:301–313
55. AL-Osta A, Alnehia A, Qaid AA, Al-Ahsab HT, Al-Sharabi A (2020) Structural, morphological and optical properties of Cr doped ZnS nanoparticles prepared without any capping agent. Optik 214:164831
56. Al-Sharabi A, Alnehia A, Al-Hammadi AH, Alhumaidha KA, A. AL-Osta, (2022) The effect of Nigella sativa seed extract concentration on crystal structure band gap and antibacterial activity of ZnS-NPs prepared by green route. J Mater Sci Mater Electron 33:20812–20822
57. Aldeen TS, Mohamed HEA, M. (2022) Maaza, ZnO nanoparticles prepared via a green synthesis approach: physical properties, photocatalytic and antibacterial activity. J Phys Chem Solids 160:110313
58. Naik EI, Naik HSB, Sarvajith MS, Pradeepa E (2021) Co-precipitation synthesis of cobalt doped ZnO nanoparticles: characterization and their applications for biosensing and antibacterial studies. Inorganic Chem Commun 130:108678
59. Shaikh S, Nazam N, Rizvi SMD, Ahmad K, Baig MH, Lee EJ, Choi I (2019) Mechanistic insights into the antimicrobial actions of metallic nanoparticles and their implications for multidrug resistance. Intl J Mole Sci 20:2468
60. Li J, Rong K, Zhao H, Li F, Lu Z, Chen R (2013) Highly selective antibacterial activities of silver nanoparticles against Bacillus subtilis. J Nanosci Nanotechnol 13:6806–6813
61. Nigussie GY, Tesfamariam GM, Tegegne BM, Weldemichel YA, Gebreab TW, Gebrehiwot DG, Gebremichel GE (2018) Antibacterial activity of Ag-doped TiO2 and Ag-doped ZnO nanoparticles. Int J Photoenergy 2018(1):1–7. https://doi.org/10.1155/2018/5927485
62. Jin T, Sun D, Su J, Zhang H, Sue HJ (2009) Antimicrobial efficacy of zinc oxide quantum dots against Listeria monocytogenes, Salmonella enteritidis, and Escherichia coli O157: H7. J food Sci 74:M46–M52
63. Premanathan M, Karthikeyan K, Jeyasubramanian K, Manivannan G (2011) Selective toxicity of ZnO nanoparticles toward Gram-positive bacteria and cancer cells by apoptosis through lipid peroxidation, Nanomedicine: Nanotechnology. Biol Med 7:184–192
64. Brayner R, Ferrari-Iliou R, Brivois N, Djediat S, Benedetti MF, Fiévet F (2006) Toxicological impact studies based on Escherichia coli bacteria in ultrafine ZnO nanoparticles colloidal medium. Nano letters 6:866–870
65. Rahman A, Harunsani MH, Tan AL, Ahmad N, Min B-K, Khan MM (2021) Influence of Mg and Cu dual-doping on phytogenic synthesized ZnO for light induced antibacterial and radical scavenging activities. Materials Science in Semiconductor Processing 128:105761
66. Inwati GK, Kumar P, Roos W, Swart H (2020) Thermally induced structural metamorphosis of ZnO: Rb nanostructures for antibacterial impacts. Colloids and Surfaces B: Biointerfaces 188:110821
67. Khan MM, Harunsani MH, Tan AL, Hojamberdiev M, Azamay S, Ahmad N (2020) Antibacterial activities of zinc oxide and Mn-doped zinc oxide synthesized using Melastoma malabathricum (L) leaf extract. Biopro Biosys Eng 43:1499–1508
68. Aklilu M, Aderaw T (2022) Khat (Catha edulis) leaf extract-based zinc oxide nanoparticles and evaluation of their antibacterial activity. J Nanomaterials 2022:10